IET Control Theory & Applications

Research Article

IET Journals
The Institution of Engineering and Technology

Saturation-aware control design for micro–nano positioning systems

ISSN 1751-8644
Received on 25th May 2017
Accepted on 3rd July 2017
E-First on 1st August 2017
doi: 10.1049/iet-cta.2017.0573
www.ietdl.org

Aurélio T. Salton[1] ✉, Ali Al-Ghanimi[2,3], Jeferson V. Flores[4], Jinchuan Zheng[3], João M. Gomes da Silva[4], Minyue Fu[5,6]

[1]*Pontifical Catholic University of Rio Grande do Sul (PUCRS), Porto Alegre - RS, Brazil*
[2]*Al-Najaf Al-Ashraf International Airport, University of Kufa, Kufa, Iraq*
[3]*School of Software and Electrical Engineering, Swinburne University of Technology, Melbourne, Victoria, Australia*
[4]*School of Engineering, Universidade Federal do Rio Grande do Sul, Brazil*
[5]*School of Electrical Engineering and Computer Science, University of Newcastle, Australia*
[6]*Department of Control Science and Engineering, Zhejiang University, Zhejiang, People's Republic of China*
✉ *E-mail: aurelio.salton@pucrs.br*

Abstract: This study proposes a non-linear saturation-aware controller for dual-stage micro–nano actuators. Dual-stage motion systems use two actuators in series in order to achieve an improved performance: a *micro actuator* responsible for a large range of actuation, and a *nano actuator* (NA) able to achieve a high bandwidth. The NA is commonly driven by flexure-based piezoelectric actuators subject to a limited range which presents large oscillations in the presence of output saturation. In order to avoid these oscillations, a non-linear smooth switching function that limits the actuation of the NA to only track references within its range is proposed. Experimental results demonstrate the effectiveness of the proposed approach, which is able to reduce oscillations and energy consumption without compromising settling time performance.

1 Introduction

A micro–nano motion system, or dual-stage actuator, is comprised of two actuators connected in series with complementary characteristics: a *micro actuator* (MA) that possesses a long action range but relatively slow response time, and a *nano actuator* (NA) that provides the system with a faster response but has a limited range of actuation. Given the significantly smaller range of actuation of the NA, a recurring problem of such systems is the output saturation of this actuator during large reference steps. This problem may be inferred from the schematic depiction of a macro–nano motion system depicted in Fig. 1*a*, whose output is subject to a limited range given by $2\bar{y}_2$. Any reference command that is given beyond this range will cause the NA to saturate its output, which may lead to oscillations that might induce heat dissipation and wearing of the flexure linkage inherent to piezoelectric actuators (commonly used in the nano stage). In the absence of NA output saturation, an improved performance is achieved by an appropriate control design able to exploit the benefits of one actuator in order to compensate the limitations of the other. As a result, the dual stage strategy became popular within high precision motion applications such as Hard Disk Drives and advanced microlithography, providing the motion systems with a significant increase in servo bandwidth and disturbance rejection. Recently, other applications have been employing some form of dual stage actuation, such as *X*–*Y* systems, nanopositioning scanners and three degree of freedom microscopes.

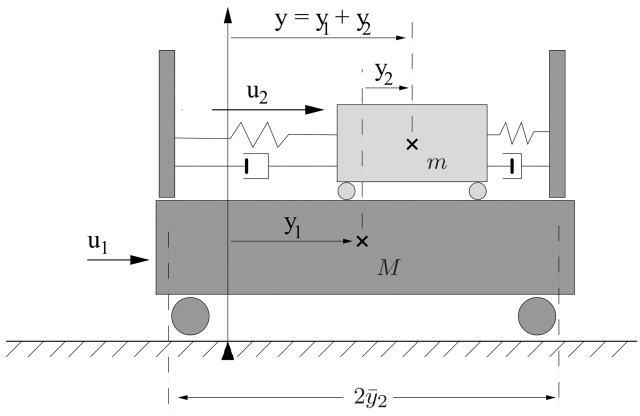

Fig. 1 *Schematic representation of a typical micro–nano actuator, respectively, represented by M and m*

Both for single- and dual-stage actuators, motion control has found countless applications and generated an equally formidable amount of breakthroughs for control theory and practise. Friction compensation [1], loop-shaping controllers [2] and saturation aware techniques [3] are some of the topics that remain of interest after many decades. While most of these methods were developed for single-input–single-output (SISO) systems, a considerable amount may be directly implemented to dual-stage (micro–nano) motion structures. The friction compensation method devised by Ruderman and Iwasaki [4] and, more generally, disturbance observers [5], are examples that may be cited. Other methods include the well known composite non-linear feedback (CNF) [6] and sliding mode techniques [7], both of which are straightforwardly extended to multi-input–multi-output (MIMO) systems.

The number of control strategies specifically designed to exploit the characteristics of dual-stage micro–nano motion systems, on the other hand, reduces drastically. An important breakthrough came in [8] where a reduced settling time was achieved by allowing the overshoot of the MA. The crucial observation being that, given the dual-stage structure of the system, it is not necessary to have both actuators at the reference in order to have the total output tracking the desired position. In fact, as long as the MA is close enough to the reference, the NA may reach it and achieve the desired tracking. A direct extension of [8] gave rise to the so-called preview control of dual-stage systems, where the MA is allowed to move ahead of time [9]. In both strategies a remarkable settling time improvement is achieved because the unique characteristics of the dual-stage structure were explicitly taken into account [10].

This paper contribution falls in the category of the latter references in that it proposes a new control strategy uniquely

© The Institution of Engineering and Technology 2017

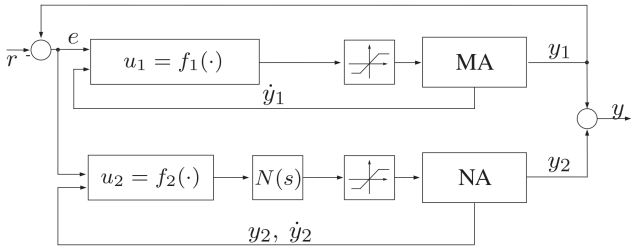

Fig. 2 *Master–slave structure representing non-linear controllers u_1 and u_2 along with the notch filter $N(s)$*

suitable for dual-stage actuators. In order to solve the output saturation problem of the NA, a non-linear control law will be proposed to activate the nano-stage only when the reference command is within reach. As such, energy consumption is significantly reduced and oscillations caused by the controller saturation are eliminated. The resulting closed-loop system comprises $\mathscr{L}_\infty$ and sector-bounded non-linearities (induced by the proposed control law) and is subject to input saturation on both actuators. Formal stability guarantees are given by a polytopic *quasi*-linear parameter varying (LPV) approach [11] combined with the absolute stability analysis of Lur'e type non-linear systems subject to saturation given in [12]. This approach is unique in the sense that it focuses on the saturation of dual-input single-output (DISO) systems with the objective of retaining both stability *and performance*. In contrast, most saturation solutions in the literature deal with SISO or MIMO systems, and are mainly focused on retaining the stability of the closed-loop system. The proposed approach is validated in a DSA comprised of a linear motor as the MA and a piezoactuated flexible structure as the NA [8]. Experimental results show a reduction both in the system input effort and in unwanted output oscillations, evidencing the performance improvements due to the proposed control scheme.

This paper is organised as follows. Section 2 describes the system at hand and the control strategy commonly employed to macro–nano positioning systems. Section 3 describes the proposed controller and frames the closed-loop system in its state-space form so that stability results may be provided in Section 4. A design procedure for the tuning of control parameters is given in Section 5 followed by experimental results demonstrating the benefits of the proposed strategy in Section 6. Final conclusions are drawn in Section 7.

Notation: v_i denotes the ith element in vector v, S_i denotes the element in position $S(i,i)$ in a diagonal matrix S and $L_{(i)}$ denotes the ith row of matrix L. $y(t)$ will be denoted only by y when its time-dependence can be inferred from the context.

2 Micro–nano motion system

2.1 System description

Consider the micro–nano actuator illustrated in Fig. 1 where the *micro actuator* (MA - also referred to as primary) is modelled by a double integrator and the *nano actuator* (NA - secondary) is represented by a mass–spring–damper system. In this case, M, $y_1(t)$ and $u_1(t)$ denote the mass, position and input of the MA and, accordingly, m, $y_2(t)$ and $u_2(t)$ are related to the NA. Also, spring and damper coefficients of the secondary are represented by k and c.

This simplified model is usually employed to describe micro–nano systems with actuators driven, respectively, by a linear motor and a piezoelectric stage. In the particular case of piezoelectric actuators, it is verified that the primary actuator is more massive than the secondary, i.e. $M >> m$, and that the secondary presents a higher bandwidth when compared to the primary. Under these conditions, the interaction between actuators is negligible and, consequently, each actuator dynamics may be given by [13]

$$\ddot{y}_1(t) = \frac{k_{v_1}}{M} u_1(t), \tag{1}$$

$$\ddot{y}_2(t) = \frac{1}{m}\big(k_{v_2} u_2(t) - k y_2(t) - c\dot{y}_2(t)\big), \tag{2}$$

where k_{v_1} and k_{v_2} are constants that transform the input signal from volts to the actual force being applied to the system. Furthermore, as depicted in Fig. 1, the output displacement of the NA is given with respect to the output of the MA. Therefore, the total displacement of the system is given by $y(t) = y_1(t) + y_2(t)$, and defines the overall output of the micro-nano. The main control objective (to be o formalised in the following sections) is to ensure that the output $y(t)$ tracks a step-like reference signal $r(t)$ as fast as possible.

2.2 Dual-stage control

The micro–nano actuator defined in (1) and (2) is a DISO system designed to exploit the benefits of the individual actuators. By coupling a long-range actuator (able to achieve a displacement of several micrometres) with a fast dynamics actuator (able to achieve a large bandwidth), an overall improved performance is expected. Since different input combinations generate the same output trajectory due to the freedom available in DISO systems, the control design of micro–nano actuators may become a challenging task [9]. A common strategy to work around this excessive freedom is given by the so-called master–slave structure, where the MA takes the role of master and tracks the reference neglecting the presence of the NA. That is, while the primary actuator control law is a function of its position, velocity and reference

$$u_1(t) = f_1(y_1(t),\ \dot{y}_1(t), r(t)),$$

the secondary depends (in addition to its own position and velocity) on the remaining tracking error defined by $e(t) = y_1(t) - r(t)$:

$$u_2(t) = f_2(e(t),\ y_2(t),\ \dot{y}_2(t))\,.$$

Hence, if reference tracking is achieved in steady state, it follows that $y_1 \to r$ and $y_2 = y_1 - r \to 0$. The master–slave structure is depicted in Fig. 2 where it is clear that the NA tracks the remaining error between the MA and the reference.

There is one additional constraint present in the secondary stage. Since this actuator is driven by a flexible structure described by (2), its limited input implies a limited output. Considering that the static gain of (2) is given by k_{v_2}/k and that $\bar{u}_2$ denotes the input limit of the NA, then the maximum displacement of the secondary actuator (ignoring possible overshoot due to the transient response) is

$$\bar{y}_2 = \frac{k_{v_2}}{k}\bar{u}_2\,. \tag{3}$$

As a consequence, when the tracking error is larger than $\bar{y}_2$, the overall system is limited by the bandwidth of the MA. Also notice that the NA loop in Fig. 2 includes a linear compensator $N(s)$ in the direct feedback path of the NA control loop. Flexible structures such as the ones used to accommodate piezoelectric actuators are commonly subject to undesired resonant peaks that might compromise the performance. Therefore, $N(s)$ represents loop shaping filters, such as notch filters, that might be used to compensate these resonant peaks allowing the system model to be simplified to (2). The experimental results considered in this paper will make use of one such compensator.

From (1), (2) and the structure depicted in Fig. 2, the following state-space representation can be considered:

$$\begin{aligned} \dot{x}(t) &= Ax(t) + B\,\mathrm{sat}_{\bar{u}}(u(t)),\\ y(t) &= Cx(t), \end{aligned} \tag{4}$$

where $x(t) \in \mathbb{R}^4$ is the state vector defined by

© The Institution of Engineering and Technology 2017

$$x(t) = \begin{bmatrix} y_1(t) - r(t) & \dot{y}_1(t) & y_2(t) & \dot{y}_2(t) \end{bmatrix}',$$

$u(t) = \begin{bmatrix} u_1(t) & u_2(t) \end{bmatrix}' \in \mathbb{R}^2$ are the inputs and

$$A = \begin{bmatrix} 0 & 1 & 0 & 0 \\ 0 & 0 & 0 & 0 \\ 0 & 0 & 0 & 1 \\ 0 & 0 & \dfrac{-k}{m} & \dfrac{-c}{m} \end{bmatrix}, \quad B = \begin{bmatrix} 0 & 0 \\ b_1 & 0 \\ 0 & 0 \\ 0 & b_2 \end{bmatrix},$$

$$C = \begin{bmatrix} 1 & 0 & 1 & 0 \end{bmatrix}$$

are the system matrices with $b_1 = k_{v_1}/M$ and $b_2 = k_{v_2}/m$. Furthermore, each control input is assumed to be limited by a symmetric saturation $-\bar{u}_1 \leq u_1(t) \leq \bar{u}_1$ and $-\bar{u}_2 \leq u_2(t) \leq \bar{u}_2$, i.e. each component of the vector $\text{sat}_{\bar{u}}(u(t))$ is defined as follows:

$$\text{sat}_{\bar{u}_j}(u(t)) = \text{sgn}(u_j(t))\min(|u_j(t)|, \bar{u}_j), \quad j = 1, 2.$$

Note that the first state in $x(t)$ corresponds exactly to the tracking error $e(t)$. Hence, the control objective is to design a $u(t)$ taking explicitly into account the saturation limits such that the origin of (4) is asymptotically stable, i.e. ensuring the reference tracking in steady state. This design problem is addressed in the following sections.

3 Dealing with saturating actuators

Besides limiting the bandwidth of the overall system, the saturation of the NA is particularly undesirable for two main reasons: unnecessary energy consumption and output oscillations. As described in the previous section, a saturated input in the NA implies a limited output displacement $\bar{y}_2$. As a result, when the MA is far from the reference, a full control input applied to the NA will not move the output any closer to the reference, i.e. energy is spent and nothing is gained in return. Furthermore, as already mentioned, flexure-based mechanisms are subject to a number of resonance peaks that are commonly compensated by notch-filters and linear compensators which are compromised in the presence of saturation, leading to significant oscillations.

This section will elaborate on a simple form of non-linear controller that avoids the saturation of the NA independently of the reference step being pursued. In general terms, the idea is to shape the reference of this stage so that it is only active in a range that does not lead to the saturation of $u_2(t)$. Since the NA tracks the remaining error between the MA and the reference, there is nothing to be gained by allowing the NA to track this error when it is larger than its range $\bar{y}_2$. This remark calls for a switching function that allows the NA to 'see' the reference only when it is sufficiently close, i.e. within its range. Furthermore, a smooth switching function should be preferred in order to avoid the excitation of higher frequencies. In what follows we make the traditional assumption that all states are known and available for both control laws.

3.1 MA control

The actions of the MA are decoupled from those of the NA by the master–slave strategy. Therefore, the control law of the MA could, in principle, take any form the designer finds suitable for the application at hand. Since this paper is focusing on the saturation of the actuators, it will be assumed that the traditional Proximate Time-Optimal Servomechanism – PTOS [14] will be the MA control law of choice. This control law is given by,

$$u_1(t) = -k_e x_1 - k_{d1} x_2 - \psi(x_1), \tag{5}$$

where

$$\psi(x_1) = \begin{cases} k_{p1} x_1, & |x_1| \leq y_l, \\ \text{sgn}(x_1)(k_{d1}\sqrt{2\alpha\bar{u}_1|x_1|b_1} + \bar{u}_1), & |x_1| > y_l, \end{cases} \tag{6}$$

where $\bar{u}_1$ is the saturation level of the primary actuator, k_e and k_{p1} are related to the proportional gain of the control law and are free parameters along with the so-called acceleration discount factor $0 < \alpha < 1$. Further conditions are imposed on the derivative gain k_{d1} and y_l so that continuity is achieved at the switching instant

$$y_l = \frac{\bar{u}}{k_{p1}}, \quad k_{d1} = \sqrt{\frac{2k_{p1}}{\alpha b_1}}. \tag{7}$$

For details on this controller the reader is invited to refer to [15] and references therein. Here it suffices to say that for $|x_1| > y_l$ a non-linear function is used to saturate the controller and allow for an aggressive approach to the reference. For $|x_1| \leq y_l$, on the other hand, the PTOS becomes a simple proportional–derivative controller, thus settling at the reference without any chattering. Gain k_e is necessary for our stability result, as will be clear in the following sections.

3.2 NA control law

The objective of this section is to devise a control law for the NA such that it only moves when the reference is close enough, and that it does not saturate, preventing the occurrence of oscillations. Both these tasks may be achieved by a switching function that allows the NA to track the reference only when it is within range. To achieve this in a smooth manner, we propose the following non-linear controller:

$$u_2 = -k_{p2}(x_3 - x_1\psi_a(x_1)) - k_{d2}x_4, \tag{8}$$

for some proportional k_{p2} and derivative k_{d2} gains and for $\psi_a(x_1)$ given by

$$\psi_a(x_1) = \frac{1 - \text{htan}(\beta_1(|x_1| - \beta_2))}{2}, \tag{9}$$

where ' htan' stands for the hyperbolic tangent. Non-linear function (9) is depicted in Fig. 3 for $x_1 > 0$ where it is clear that for large values of x_1, $\psi_a(x_1)$ is approximately zero. This means that for large reference errors the NA does not attempt to track the error between the reference and the MA (recall that $x_1 := y_1 - r$). However, as the primary actuator reaches the reference and the value of x_1 diminishes, the non-linear function $\psi_a(x_1)$ approaches one, and the NA actuator smoothly tracks the remaining difference between y_1 and r. This control law, therefore, is a smooth switching function that limits the actuation of the secondary actuator so that it does not saturate. With appropriate choices of β_1, which determines the slope of the curve in Fig. 3, and β_2, which determines its horizontal offset, it is straightforward to achieve this smooth transition between $u_2 \simeq -k_{p2}x_3 - k_{d2}x_4$ and

$$u_2 \simeq -k_{p2}(x_3 - x_1) - k_{d2}x_4.$$

As a consequence, the saturation of this actuator is avoided for any reference level, and oscillations are reduced along with energy consumption.

Remark 1: In order to design $\psi_a(x_1)$ defined in (9) and depicted in Fig. 3, one must choose the parameters β_1 and β_2 such that $\psi_a(x_1) \simeq 1$ in the range $\bar{y}_2$ of the NA. This is easily achieved by noticing that the maximum slope of this curve occurs at $x_1 = \beta_2$ and is given by $-\beta_1/2$. By tracing the resulting tangent line (dashed black line) two conclusions follows:

1. The interception of the tangent line with $\psi_a(x_1) = 1$ occurs at $x_1 = \beta_2 - 1/\beta_1$, leading to the approximation

© The Institution of Engineering and Technology 2017

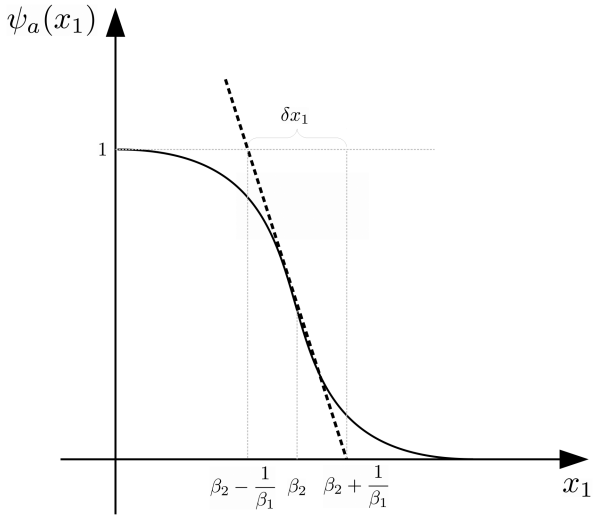

Fig. 3 *Illustration of non-linear function $\psi_a(x_1)$ used to limit the actuation of the secondary actuator*

$$\psi_a(x_1) \simeq 1, \quad \text{for } |x_1| < \beta_2 - \frac{1}{\beta_1}. \tag{10}$$

2. The interception of the tangent line with $\psi_a(x1) = 1$ occurs at $x_1 = \pm\beta_2 \pm 1/\beta_1$, leading to the approximation

$$\psi_a(x_1) \simeq 0, \quad \text{for } |x_1| > \beta_2 + \frac{1}{\beta_1}. \tag{11}$$

Note that the desired transition interval δx_1 defining the region between $\psi_a(x_1) \simeq 0$ and $\psi_a(x_1) \simeq 1$ is given by

$$\delta x_1 = \beta_2 + \frac{1}{\beta_1} - \left(\beta_2 - \frac{1}{\beta_1}\right) = \frac{2}{\beta_1}.$$

Also note that ideally $\psi_a(x_1) \simeq 1$ when the tracking error lies within the NA range $\bar{y}_2$, which results in $\bar{y}_2 = \beta_2 - 1/\beta_1$. Based on this reasoning it readily follows that for a given $\bar{y}_2$ and δx_1, β_1 and β_2 must be chosen as

$$\beta_1 = \frac{2}{\delta x_1}, \quad \beta_2 = \bar{y}_2 + \frac{1}{\beta_1}. \tag{12}$$

Based on the formulation presented in this section, it is clear that control laws (5) and (8) are based on the feedback of x_1, x_2, x_3 and x_4, i.e. we suppose that all system states are measurable.

3.3 Closed-loop system

Given the individual controllers defined in the previous sections, the combined control input may be expressed as follows:

$$\begin{bmatrix} u_1 \\ u_2 \end{bmatrix} = \begin{bmatrix} -k_e & -k_{d1} & 0 & 0 \\ -k_{p2}\psi_a(x_1) & 0 & -k_{p2} & -k_{d2} \end{bmatrix} x - \begin{bmatrix} 1 \\ 0 \end{bmatrix} \psi(x_1), \tag{13}$$

which is equivalent to

$$u = K(x_1)x - B_\psi \psi(x_1), \tag{14}$$

with $B_\psi = [1\,0]'$. In this form, it is clear that $\psi_a(x_1)$ performs a scheduling in the state feedback gain, represented by $K(x_1)$, in order to avoid the saturation of the NA, while $\psi(x_1)$ is responsible to provide near time-optimal performance to the MA.

Both actuators are subject to control saturation which will be dealt with by means of the decentralised deadzone non-linearity $\phi(u)$ given by

$$\phi(u) = u - \text{sat}_{\bar{u}}(u). \tag{15}$$

Hence, from (4), (14) and (15), the closed-loop system can be rewritten as follows:

$$\dot{x} = (A + BK(L_c x))x - \bar{B}\psi(L_c(x)) - B\phi(u) \tag{16}$$

with $L_c = [1\,0\,0\,0]$ and $\bar{B} = BB_\psi$.

4 Stability results

Based on the state-space representation (16), obtained by the application of control laws (5) and (8) into (4), we provide in this section a result that allows the assessment of the regional asymptotic stability of the closed-loop system. Hence, once the gains k_e, k_{p1}, k_{d1}, k_{p2}, k_{d2} and the parameters of non-linearities ψ and ψ_a have been computed, it is possible to certify that the origin of (16) is asymptotically stable, which implies that the tracking is guaranteed provided that the initial states are in a well characterised ellipsoidal region around the origin.

The proposed stability conditions will be based on the following properties:

1. $\psi_a(L_c x)$ is an $\mathscr{L}_\infty$ bounded function and consequently a quasi-LPV approach [16] can be employed to represent $K(L_c x)$.
2. $\psi(L_c x)$ is a sector bounded non-linearity (see Fig. 5) for a particular range of $L_c x$ [17], i.e. it satisfies a sector condition locally, and therefore the classical absolute stability theory [18] can be applied.
3. $\text{sat}_{\bar{u}}(u)$ was rewritten as a deadzone non-linearity which satisfies the generalised sector approach proposed in [19].

While each point above will be individually addressed by a specific lemma, the proof of each lemma is omitted since they can be derived from the results in [16, 18, 19], respectively.

Lemma 1: Consider a continuously differentiable non-linear function $\psi_a(L_c x)$ such that $0 \le \psi_a(L_c x) \le 1$, $\forall L_c x$. Then $K(L_c x) = K(x_1)$ in (14) can be written by a combination of vertices $\{K_1, K_2\}$ such that

$$K(L_c x) = \sum_{j=1}^{2} q_j K_j, \quad 0 \le q_j \le 1, \quad \sum_{j=1}^{2} q_j = 1 \tag{17}$$

with

$$K_1 = \begin{bmatrix} -k_e & -k_{d1} & 0 & 0 \\ 0 & 0 & -k_{p2} & -k_{d2} \end{bmatrix}, \quad K_2 = \begin{bmatrix} -k_e & -k_{d1} & 0 & 0 \\ -k_{p2} & 0 & -k_{p2} & -k_{d2} \end{bmatrix}. \tag{18}$$

Assuming now that $\psi(L_c x)$ is locally confined to the sector $\nu_{\min} L_c x \le \psi(L_c x) \le \nu_{\max} L_c x$ for all $|L_c x| \le \rho, \rho > 0$. Then it follows that (16) is equivalent to

$$\dot{x} = (A + BK_c(L_c x))x - B\phi(u) - \bar{B}\psi_c(L_c x) \tag{19}$$

with

$$u = K_c(L_c x)x - B_\psi \psi_c(L_c x), \tag{20}$$

$K_c(L_c x) = K(L_c x) - B_\psi \nu_{\min} L_c$ and

$$\psi_c(L_c x) = \psi(L_c x) - \nu_{\min} L_c x. \tag{21}$$

From (17), it follows that

$$K_c(L_c x) = \sum_{j=1}^{2} q_j K_{cj}, \quad 0 \le q_j \le 1, \quad \sum_{j=1}^{2} q_j = 1 \tag{22}$$

© The Institution of Engineering and Technology 2017

with $K_{cj} = K_j - B_\psi \nu_{\min} L_c$.

In this case, provided $|L_c x| \leq \rho$, we have $\psi_c(L_c x)$ bounded by sector $[0, \nu_c]$ where $\nu_c = \nu_{\max} - \nu_{\min}$ and the following lemma can be stated.

Lemma 2: Consider $\psi_c(L_c x)$ defined in (21). Thus the sector condition

$$\psi_c(L_c x)\eta(\psi_c(L_c x) - \nu_c L_c x) \leq 0, \quad \eta > 0 \tag{23}$$

is satisfied locally in the set

$$\mathcal{S}_c = \left\{ x \in \mathbb{R}^4; |L_c x| \leq \rho \right\}. \tag{24}$$

Lemma 3: Consider system (19) and the control input (20). If $x(t) \in \mathcal{S}$ with

$$\begin{aligned} \mathcal{S} = \{ x \in \mathbb{R}^4; |(K_{c(i)}(L_c x) - H_{(i)})x \\ -(B_{\psi i} + N_i)\psi_c(L_c x)| \leq \bar{u}_i, i = 1, 2 \} \end{aligned} \tag{25}$$

then the generalised sector condition

$$\phi(u)' T(\phi(u) - Hx - N\psi_c(L_c x)) \leq 0 \tag{26}$$

is satisfied for any diagonal positive definite matrix $T \in \mathbb{R}^{2\times 2}$.

Note that in the above $H \in \mathbb{R}^{2\times 4}$ and $N = [n_1\, n_2]' \in \mathbb{R}^{2\times 1}$ are free variables to be determined.

Based on Lemmas 1–3 the following theorem can be stated regarding the stability of (19) under control law (20).

Theorem 1: Suppose that K_{cj}, $j = 1, 2$ are such that $\mathbb{A}_j = A + BK_{cj}$ are Hurwitz. If there exist a symmetric positive definite matrix $W \in \mathbb{R}^{4\times 4}$, a diagonal positive definite matrix $S \in \mathbb{R}^{2\times 2}$, matrices $X \in \mathbb{R}^{2\times 4}$, $\Gamma \in \mathbb{R}^{2\times 1}$ and a positive scalar $\bar{\eta}$ such that the following linear matrix inequalities (LMIs) are verified:

$$\begin{bmatrix} \mathbb{A}_j W + W\mathbb{A}_j' & -\bar{B}\bar{\eta} + WL_c'\nu_c & -BS + X' \\ * & -2\bar{\eta} & \Gamma' \\ * & * & -2S \end{bmatrix} < 0, \quad j = 1, 2 \tag{27}$$

$$\begin{bmatrix} W & -WL_c'\nu_c & WK_{cj(i)}' - X_{(i)}' \\ * & 2\bar{\eta} & -\bar{\eta}B_{\psi i} - \Gamma_i \\ * & * & \bar{u}_i^2 \end{bmatrix} > 0 \begin{matrix} i = 1, 2 \\ j = 1, 2 \end{matrix} \tag{28}$$

$$\begin{bmatrix} W & WL_c' \\ * & \rho^2 \end{bmatrix} > 0 \tag{29}$$

then the trajectories of closed-loop system (19) and (20) starting in the ellipsoidal set

$$\mathcal{E}(W^{-1}, 1) = \{ x \in \mathbb{R}^4; x' W^{-1} x \leq 1 \},$$

remain bounded to this set and converge asymptotically to the origin.

The proof of Theorem 1 can be derived from Lemmas 1–3 following the same procedure presented in [20]. Also, note that the proportional gain k_e was introduced in order to satisfy the assumption that $\mathbb{A}_j = A + BK_{cj}$, $j = 1, 2$ are Hurwitz, otherwise $\mathbb{A}_1$ would always present an eigenvalue at the origin and (27) would not be feasible.

5 Design procedure

The framework proposed in the previous sections can be implemented in two distinct phases: first, controller gains must be determined to obtain a desired closed-loop behaviour and then a stability analysis is performed to ensure that the closed-loop system is stable for a desired set of reference steps. In the sequel, we will provide a systematic procedure to be performed in each phase.

5.1 Controller design

From the reasoning presented in Section 3, it follows that $\psi_a(x_1) \simeq 1$ for $|x_1| \leq y_l$ and then $u_1 = [-(k_e + k_{p1}) - k_{d1}\, 0\, 0]$ and $u_2 = [-k_{p2}\, 0 - k_{p2} - k_{d2}]$ such that the closed-loop behaviour of each actuator is given by

$$G_{MA}(s) = \frac{Y_1(s)}{R(s)} = \frac{(k_e + k_{p1})b_1}{s^2 + k_{d1}b_1 s + (k_{p1} + k_e)b_1},$$

$$G_{NA}(s) = \frac{Y_2(s)}{X_1(s)} = \frac{b_2 k_{p2}}{s^2 + (k_{d2}b_2 + (c/m))s + \left(k_{p2}b_2 + (k/m)\right)},$$

respectively. Hence, considering a desired second-order behaviour for $G_{MA}(s)$ and $G_{NA}(s)$ given by damping coefficients ξ_1 and ξ_2, and natural frequencies ω_1 and ω_2, then, gains k_{p1}, k_{d1}, k_{p2} and k_{d2} can be computed as follows:

$$\begin{aligned} k_{p1} + k_e &= \frac{\omega_1^2}{b_1}, \qquad k_{d1} = \frac{2\xi_1\omega_1}{b_1}, \\ k_{p2} &= \frac{1}{b_2}\left(\omega_2^2 - \frac{k}{m}\right), \quad k_{d2} = \frac{1}{b_2}\left(2\xi_2\omega_2 - \frac{c}{m}\right). \end{aligned} \tag{30}$$

Thus, the proposed controller can be designed in the following manner:

Step 1: Choose ξ_1, ξ_2, ω_1 and ω_2 to obtain a desired closed-loop response. With $k_e = 0.1 \cdot k_{p1}$ determine k_{p1}, k_{d1}, k_{p2} and k_{d2} from (30).

Step 2: Determine β_1 and β_2 from Remark 1 such that the NA only tracks the reference when it is within range and that no saturation occurs.

Remark 2: Since k_e was introduced only for stability purposes, this gain should be tuned to minimise its effect on the closed-loop performance. Our experience shows that a k_e around 10% of k_{p1} is enough to guarantee the closed-loop stability without compromising the MA performance.

5.2 Stability analysis

With the controller designed following the procedure in the previous section, closed-loop stability can be verified as follows:

Step 1: Choose $\nu_{\max}$ tangent to $\psi_c(L_c x)$ at the origin and $\nu_{\min}$ such that the sector condition is satisfied for ρ greater than the maximum reference step and determine K_j and K_{cj}, $j = 1, 2$ as in (17) and 22, respectively, such that matrices $\mathbb{A}_1$ and $\mathbb{A}_2$ are Hurwitz.

Step 2: Solve the optimisation problem

$$\text{OP: } \max \ \text{trace}\{W\} \text{ subject to } (27) - (29).$$

Step 3: If optimisation problem is not feasible, increase k_e and go back to Step 2.

Remark 3: It should be pointed out that Step 2 is a stability test and is performed off-line. Note also that OP is a convex optimisation problem, since it involves a linear criterion and LMIs constraints, thus, efficient numerical packages are available to solve it (see for instance [21]. Furthermore, in addition to the asymptotic stability of the origin (which is guaranteed by the satisfaction of LMIs (27)–(29)) this step provides a maximised region of admissible states. The designer should therefore verify if the physical range of operation of the system is included in this region. In the cases that

© The Institution of Engineering and Technology 2017

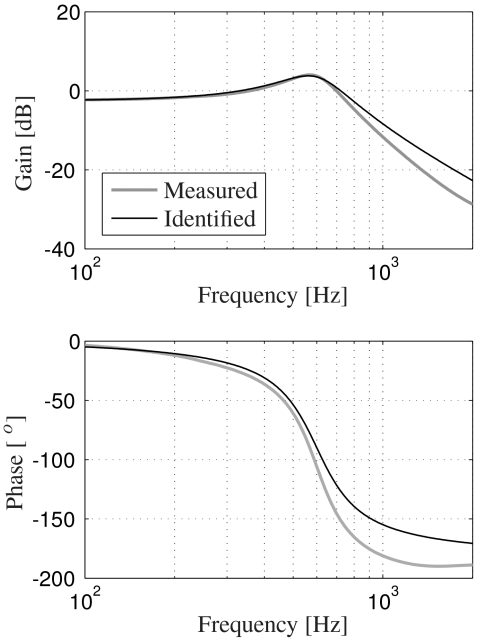

Fig. 4 *Measured and identified Bode diagrams of the NA*

Table 1 System parameters

Parameter	Value	Units
b_1	1.5699×10^7	$[\mu\text{m/s}^2\text{V}]$
b_2	1.07×10^7	$[\mu\text{m/s}^2\text{V}]$
k/m	1.4212×10^7	$[\text{s}^{-2}]$
c/m	1.885×10^3	$[\text{s}^{-1}]$
$\bar{u}_1$	8	[V]
$\bar{u}_2$	3	[V]

it is not, a re-tuning of the control law parameters should be performed.

6 Experimental results

In our experimental results, we have implemented control laws (5) and (8) on the macro–nano actuator presented in [9]. The MA is effectively modelled as a double integrator as in (1) and the NA is modelled as a mass–spring–damper according to (2). While the system parameters identified from the experimental setup are given in Table 1, Fig. 4 shows Bode plots of the NA, where the light grey line is the measured frequency response and the dark line is the identified model.

In order to fully illustrate the benefits of the proposed controller we have damped the NA frequency response with a notch filter given by

$$N(s) = \frac{s^2 + 2\zeta_1\omega_{ch}s + \omega_{ch}^2}{s^2 + 2\zeta_2\omega_{ch}s + \omega_{ch}^2} \tag{31}$$

with $\zeta_1 = 0.1$, $\zeta_2 = 0.5$, $\omega_{ch} = 600 \cdot 2\pi$ rad/s, tuned based on the frequency response presented in Fig. 4. As a result, the system that is effectively controlled by (8) is given by the combination of the notch filter in (31) and the dynamic equation in (2). The resulting control structure is depicted in the schematic of Fig. 2 and was implemented with a sampling frequency of 10 kHz. By applying the tuning Steps 1 and 2 presented in Section 5.1, the following control parameters are obtained:

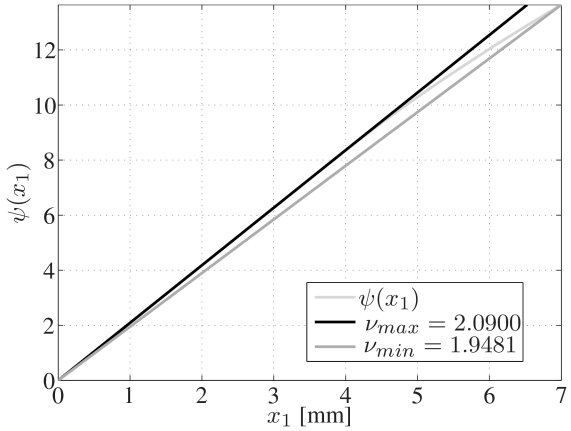

Fig. 5 *Non-linear function $\psi(x_1)$ given by (6) with a local sector defined as $[\nu_{\min}, \nu_{\max}] = [1.9481, 2.0900]$*

$$\begin{aligned} k_{p1} &= 2.09, & k_{d1} &= 1.72 \times 10^{-2}, \\ k_e &= 0.25, & \alpha &= 0.9, \\ k_{p2} &= 0.4, & k_{d2} &= 1 \times 10^{-5}, \\ \beta_1 &= 100\,\mu\text{m}^{-1}, & \beta_2 &= 10\,\mu\text{m}. \end{aligned} \tag{32}$$

Parameters β_1 and β_2 were tuned according to Remark 1 given that $\bar{y}_2 = 9\,\mu$m.

We may now assess the stability of this controller by performing the steps given in Section 5.2. For such, we have chosen $\nu_{\max} = 2.0900$ and $\nu_{\min} = 1.9481$ so that $\rho = 7$ mm. The sector formed by these values, along with the non-linear function $\psi(L_c x)$, is plotted in Fig. 5.

Given the control gains and the sector limits, we are now able to solve the optimisation problem given in *Step 3* of Section 5.2. Numerical results were obtained from Matlab R2011b with Yalmip [21] and the solver LMILab [22]. The optimisation problem gives

$$W^{-1} = \begin{bmatrix} 2.5893 \times 10^{-2} & 6.1619 \times 10^{-5} & \cdots & \cdots & 5.8936 \times 10^{-5} & 1.7424 \times 10^{-8} \\ 6.1619 \times 10^{-5} & 9.3250 \times 10^{-7} & \cdots & \cdots & 4.7097 \times 10^{-9} & 8.3619 \times 10^{-12} \\ 5.8936 \times 10^{-5} & 4.7097 \times 10^{-9} & \cdots & \cdots & 1.7619 \times 10^{-4} & 3.8852 \times 10^{-8} \\ 1.7424 \times 10^{-8} & 8.3619 \times 10^{-12} & \cdots & \cdots & 3.8852 \times 10^{-8} & 5.8569 \times 10^{-11} \end{bmatrix}, \tag{33}$$

and $\text{trace}\{W\} = 5.0164 \times 10^8$. It is important to mention that we can determine the maximum allowable value of $x_1 = y_1 - r$ by computing $[x_{1\max}\,0\,0\,0]W^{-1}[x_{1\max}\,0\,0\,0]' = 1$. From matrix W above it follows that $x_{1\max} = 6.2145$ mm.

Given this stability result, we have performed several experiments tracking reference steps below 75 μm. In particular, Figs. 6*a* and *b*, respectively, show the system response to a step reference of 70 μm when subject to the a linear controller, i.e. $\psi_a(x_1) = 1$, and to the proposed controller. The proposed controller shows clear advantages over its linear counterpart, in fact, the linear controller in Fig. 6*a* shows a classical response of micro–nano actuators tracking large reference steps: the NA rushes ahead towards the reference only to saturate immediately after, causing oscillations on the system that might induce heat dissipation and wearing of the flexure linkage. Furthermore, no performance improvement is achieved by this action of the NA, the system must wait for the MA to be close enough to the reference so that the effects of the NA are relevant for the tracking performance.

Fig. 6*b*, on the other hand, shows the benefits of the proposed non-linear control law. Note that the NA does not reach its full saturation limit and, therefore, does not induce oscillations to the

© The Institution of Engineering and Technology 2017

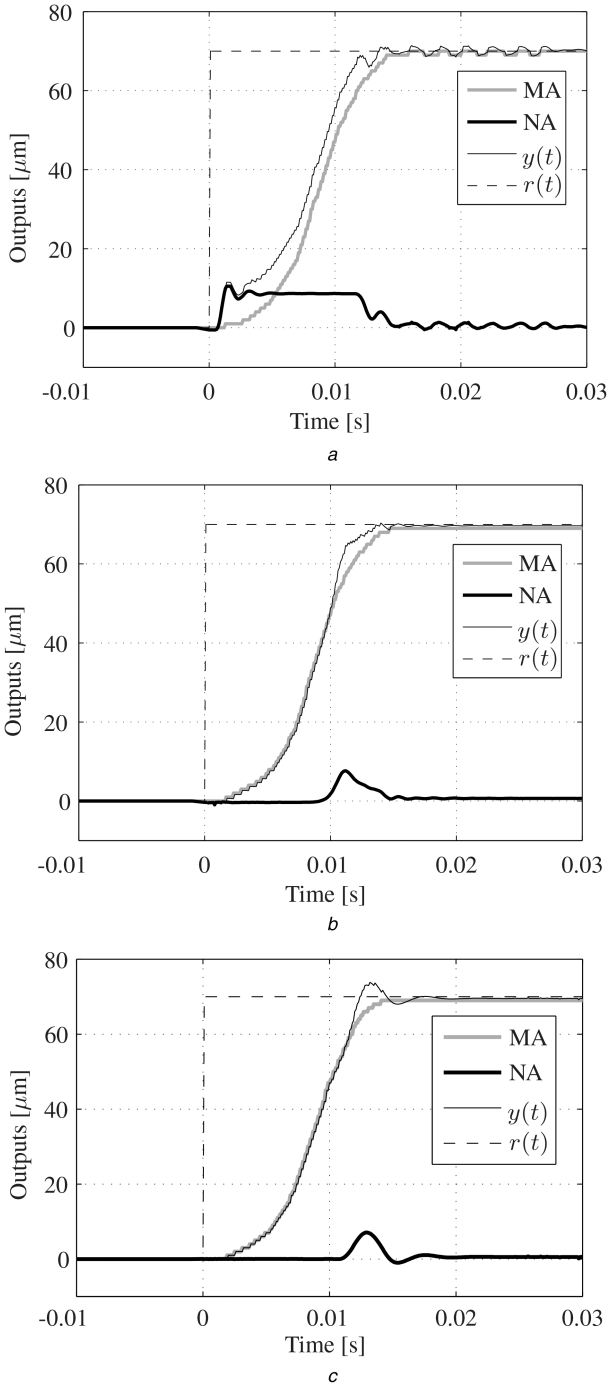

Fig. 6 *Experimental results tracking a* 70 μm *step*
(a) System response for u_1 given by PTOS and u_2 by linear feedback. The oscillations are a result of the saturation of u_2, ***(b)*** System response for u_1 given by PTOS and u_2 by (8). The oscillations are avoided since the NA never reached its output saturation limit, ***(c)*** System response for u_1 given by PTOS and u_2 by hard switching. The oscillations are avoided but the settling time is compromised

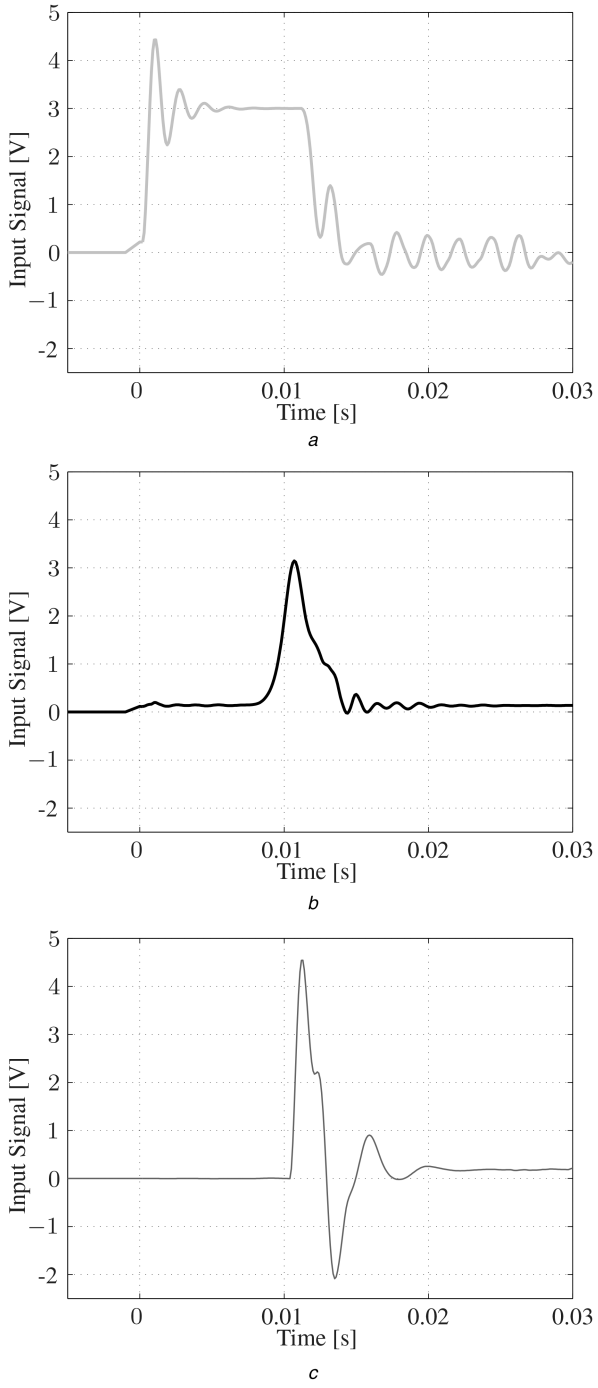

Fig. 7 *Experimental results: input signals of the NA for* u_2
(a) Linear feedback, ***(b)*** Proposed controller, ***(c)*** Hard switching

system output. For further comparison purposes, Fig. 6*c* shows the system response when a hard switching is applied, i.e. $\psi_a(x_1) = 1$ for $|x_1| < 9\,\mu$m and $\psi_a(x_1) = 0$ otherwise. The figure shows that this hard switching approach induces oscillations to the system and compromises the settling time performance. Furthermore, while the tracking performance is improved by the proposed controller, its energy consumption is significantly smaller than that of the comparative methods. A measure of the $\mathscr{L}_2$ norm of the input u_2 of the NA presented in Fig. 7 shows that the linear controller results in $\| u_{2l} \| = 32.8$, while the non-linear controller reduces this value to $\| u_{2nl} \| = 12.7$, i.e. less than 39% of the energy is used without compromising the performance. Clearly, the larger the step reference the bigger the energy consumption of the linear controller. There is also a significant energy consumption reduction when the smooth switching law is compared to the hard switching approach which consumes $\| u_{2hs} \| = 15.6$ V. As a result, the hard switching strategy consumes over 22% more energy than the proposed approach.

7 Conclusion

This paper proposed a smooth non-linear function to be applied to the NA control law in order to reduce oscillations caused by input saturation. By preventing this actuator from reaching its input limit, loop shaping compensators, such as notch filters, are always active during the tracking phase. As a consequence, resonant peaks are not excited in the presence of large reference steps and oscillations otherwise induced by these peaks vanish. Since it is always a difficult task to tune non-linear controllers, a methodology for finding the smooth non-linear function parameters was also presented. Furthermore, thorough stability results were developed

© The Institution of Engineering and Technology 2017

such that the closed-loop stability under the proposed control scheme is guaranteed. The overall improvements provided by the proposed approach were shown experimentally. In fact, experimental results demonstrated that the proposed controller is able to achieve a less oscillatory response – reducing heat dissipation and fatigue of the flexure hinge – when compared to traditional linear controllers. Furthermore, by limiting the actuation of the NA so it only attempts to track references within its reach, a significant reduction of control effort is achieved without settling time degradation. It remains as future work the investigation of the proposed strategy when the NA is subject to an integrator term. In this scenario, an anti-windup scheme will have to be implemented, which poses an extra challenge for the stability analysis inasmuch as applying anti-windup schemes to non-linear controllers is not a trivial task [23].

8 Acknowledgments

This work was partially supported by CNPq grants 309272/2015-7 (A.T. Salton) and 43979/2014-6, 305886/2015-0 (J.V. Flores).

9 References

[1] Chong, S.H., Sato, K.: 'Practical and robust control for precision motion: AR-CM NCTF control of a linear motion mechanism with friction characteristics', *IET Control Theory Appl.*, 2015, **19**, (5), pp. 745–754

[2] Yang, J., Zhu, Y., Yin, W.*, et al.*: 'LFT structured uncertainty modeling and robust loop-shaping controller optimization for an ultraprecision positioning stage', *IEEE Trans. Ind. Electron.*, 2014, **61**, (12), pp. 7013–7025

[3] Xu, Q.: 'Piezoelectric nanopositioning control using second-order discrete-time terminal sliding-mode strategy', *IEEE Trans. Ind. Electron.*, 2015, **62**, (12), pp. 7738–7748

[4] Ruderman, M., Iwasaki, M.: 'Observer of nonlinear friction dynamics for motion control', *IEEE Trans. Ind. Electron.*, 2015, **62**, (9), pp. 5941–5949

[5] Back, J., Shim, H.: 'Reduced-order implementation of disturbance observers for robust tracking of non-linear systems', *IET Control Theory Appl.*, 2014, **19**, (17), pp. 1940–1948

[6] Lin, Z., Pachter, M., Banda, S.: 'Toward improvement of tracking performance nonlinear feedback for linear systems', *Int. J. Control*, 1998, **70**, (1), pp. 1–11

[7] Xu, B., Zhou, D., Sun, S.: 'Finite time sliding sector guidance law with acceleration saturation constraint', *IET Control Theory Appl.*, 2016, **10**, (7), pp. 789–799

[8] Zheng, J., Fu, M.: 'Nonlinear feedback control of a dual-stage actuator system for reduced settling time', *IEEE Trans. Control Syst. Technol.*, 2008, **16**, (4), pp. 717–725

[9] Salton, A.T., Chen, Z., Zheng, J.*, et al.*: 'Constrained optimal preview control of dual-stage actuators', *IEEE/ASME Trans. Mechatronics*, 2016, **21**, (2), pp. 1179–1184

[10] Salton, A.T.: '*High performance dual-stage systems, control and design*' (Verlag Dr. Müler, Saarbrücken, 2011)

[11] Wu, F., Lin, Z., Zheng, Q.: 'Output feedback stabilization of linear systems with actuator saturation', *IEEE Trans. Autom. Control*, 2007, **52**, (1), pp. 122–128

[12] Gomes da Silva, J.M.Jr., , Castelan, E.B., Corso, J.*, et al.*: 'Dynamic output feedback stabilization for systems with sector-bounded nonlinearities and saturating actuators', *J. Franklin Inst.*, 2013, **350**, (3), pp. 464–484

[13] Zheng, J., Salton, A., Fu, M.: 'Design and control of a rotary dual-stage actuator positioning system', *IEEE/ASME Trans. Mechatronics*, 2011, **21**, (6), pp. 1003–1012

[14] Workman, M., Kosut, R., Franklin, G.: 'Adaptive proximate time-optimal servomechanisms: discrete-time case'. Proc. 26th IEEE Conf. Decision and Control, 1987, pp. 1548–1553

[15] Salton, A.T., Chen, Z., Fu, M.: 'Improved control design methods for proximate time-optimal servomechanisms', *IEEE/ASME Trans. Mechatronics*, 2012, **17**, (6), pp. 1049–1058

[16] De Oliveira, M.C., Geromel, J.C., Hsu, L.: 'LMI characterization of structural and robust stability: the discrete-time case', *Linear Algebr. Appl.*, 1999, **296**, (1), pp. 27–38

[17] Flores, J.V., Neto, N.B., Salton, A.T.*, et al.*: 'Acceleration enhancement factor for damped systems subject to the discrete proximate time-optimal servomechanism'. Proc. 52nd IEEE Conf. Decision and Control, 2013, pp. 5137–5142

[18] Khalil, H.: '*Nonlinear systems*' (Prentice-Hall, Upper Saddle River, NJ, 2002, 3rd edn.)

[19] Gomes da Silva, J.M.Jr., , Tarbouriech, S.: 'Anti-windup design with guaranteed regions of stability: an LMI-based approach', *IEEE Trans. Autom. Control*, 2005, **50**, pp. 106–111

[20] Salton, A.T., Flores, J.V., Gomes da Silva, J.M.Jr.*, et al.*: 'A framework for the nonlinear control of dual-stage systems', *IFAC Proc. Volumes*, 2014, **47**, (3), pp. 1140–1145

[21] L"ofberg, J.: 'YALMIP: a toolbox for modeling and optimization in MATLAB'. Proc. the CACSD Conf., Taipei, Taiwan, 2004

[22] Gahinet, P., Nemirovskii, A.: '*LMI lab: a package for manipulating and solving LMIs*' (The Mathworks, South Natick, MA, 1994)

[23] Herrmann, G., Hredzak, B., Turner, M.C.*, et al.*: 'Discrete robust anti-windup to improve a novel dual-stage large-span track-seek/following method', *IEEE Trans. Control Syst. Technol.*, 2008, **16**, (6), pp. 1342–1351

© The Institution of Engineering and Technology 2017